VIEILLISSEMENT ENTRE 300 ET 450 °C D'ACIERS INOXYDABLES MARTENSITIQUES CORROYES CONTENANT 13 A 17 % DE CHROME

AGING BETWEEN 300 AND 450 °C OF WROUGHT MARTENSITIC 13-17 wt-% Cr STAINLESS STEELS

EDF
Electricité de France

Direction des Etudes et Recherches

SERVICE RÉACTEURS NUCLÉAIRES ET ECHANGEURS
Département Etude des Matériaux

Juin 1993

YRIEIX B.
GUTTMANN M.

VIEILLISSEMENT ENTRE 300 ET 450 °C D'ACIERS INOXYDABLES MARTENSITIQUES CORROYES CONTENANT 13 A 17 % DE CHROME

AGING BETWEEN 300 AND 450 °C OF WROUGHT MARTENSITIC 13-17 wt -% Cr STAINLESS STEELS

Pages : 14

93NB00106

Diffusion : J.-M. Lecœuvre
EDF-DER
Service IPN, Département SID
1, avenue du Général-de-Gaulle
92141 Clamart Cedex

© Copyright EDF 1993

ISSN 1161-0611

SYNTHÈSE :

Des aciers inoxydables martensitiques de 13 à 17 % de chrome avec ou sans nickel et avec ou sans additions durcissantes ont été vieillis entre 300 et 450 °C pendant des durées allant jusque 30 000 h. Le vieillissement se manifeste, pour tous les aciers, par une fragilisation corrélée à un durcissement d'autant plus intense et rapide que la teneur en chrome plus molybdène est élevée. Deux aciers présentent, en outre, une fragilisation de revenu réversible au cours des vieillissements à 400 °C ; une telle fragilisation n'est pas à craindre en service jusqu'à 300 °C. Un modèle de prévision des propriétés mécaniques de ces aciers en fonction des conditions de vieillissement est proposé.

93NB00106

EXECUTIVE SUMMARY :

Martensitic stainless steels containing 13-17 wt-% Cr, some also containing nickel and some having precipitation hardening additions, have been aged between 300 and 450 °C for times up to 30 000 h. For all the steels examined, the aging response takes the form of an increase of strength and hardness, correlated with embrittlement. The rate and intensity of aging increase with increasing chromium and molybdenum concentrations. In addition, two steels exhibit some temper embrittlement on long term aging at 400 °C ; such embrittlement of these materials is not expected in service at temperatures up to 300 °C. A general method of prediction of the mechanical properties of these steels as a function of aging conditions is proposed.

Aging between 300 and 450°C of wrought martensitic 13–17 wt-%Cr stainless steels

B. Yrieix and M. Guttmann

Introduction

Martensitic stainless steels are widely used for the adequate corrosion resistance associated with their good mechanical properties. In particular, these steels are utilised in the fabrication of many parts in electric power stations: pump shafts, fasteners, valve parts, turbine blades, geothermic power plant rotor, etc. Such equipment is in service for very long times at temperatures sometimes in excess of 250°C. In these conditions, such steels could become embrittled by precipitation of the chromium rich α' phase *due to their relatively high chromium content.*

Although α' embrittlement has been widely studied in ferritic stainless steels and is known to occur at relatively high temperatures (i.e. 450–520°C) in martensitic steels,[1–3] comparatively little work has been carried out on the risk of long term embrittlement of the latter via this mechanism at lower temperatures. In a recent investigation of the aging response of various steels containing 13–16 wt-%Cr, aged for up to 10 000 h between 300 and 450°C, Meyzaud and Cozar[4] have illustrated the wide variety of behaviour of these materials, depending on their chemical composition. They have proposed a model to predict the maximum evolution of their mechanical properties as a function of their metallurgical parameters. In view of this variety of behaviour and of the need to guarantee the integrity of the components up to the expected service life of pressurised water reactor (PWR) nuclear power plant (i.e. ~300 000 h), a systematic investigation of the aging behaviour of these materials held for very long times (up to 70 000 h) at temperatures between 300 and 450°C has been undertaken by Electricité de France (EDF) to check the validity of the existing predictive model or to develop a new model in the above conditions. Also, the possible occurrence of intergranular reversible temper embrittlement in these materials has been recognised.[5–6] Hence, it was deemed necessary to precisely determine the conditions of its occurrence in the various materials considered, so as to distinguish between the contributions of the two embrittling mechanisms (intragranular α' precipitation and intergranular segregation of impurities) to the overall embrittlement observed.

Table 1 Chemical composition of steels, wt-%

Designation	C	P	S	Cr	Mo	Ni	Other
Plain 13%Cr							
13Cr (A)	0·116	0·015	0·005	12·65	0·03	0·12	
13Cr (B)	0·100	0·019	0·026	12·60	0·04	0·27	
13Cr–1Ni							
13–1	0·104	0·012	0·011	12·55	0·31	1·42	
13Cr–4Ni							
13–4	0·051	0·025	0·015	13·19	0·57	4·16	
16Cr–4Ni–Mo							
16–4	0·051	0·028	0·001	15·95	1·18	4·65	
17Cr–4Ni–Cu							
17–4 PH	0·049	0·022	<0·001	16·15	0·06	4·65	3·43%Cu, 0·33%Nb

Materials

Six industrial products, containing between 13 and 17%Cr, have been studied. Some of them also contain nickel and some precipitation hardening additions. The detailed characterisation (chemical analysis, mechanical tests, microstructural, microanalytic, and fractographic examination, and determination of transformation points), as well as the study of the influence of heat treatment on the microstructure, is given elsewhere.[9] Table 1 gives the chemical composition of the materials studied.

Heat treatments are given in Table 2. The tempering temperatures of the 4%Ni steels are intercritical (i.e. between the transformation points Ac_1 and Ac_3); therefore, as shown in Table 3, the microstructure of these steels contains several per cent of reverted austenite.

In the initial unaged condition the microstructure of all the steels studied is essentially tempered lath martensite having a prior austenitic grain size between ASTM no. 4 (13–4) and 11–12 (17–4 PH). Reverted austenite and δ ferrite contents, as well as the eventual other phases present, are given in Table 3. Table 4 gives the hardness, tensile, and Charpy V-notch properties in the initial condition.

Table 2 Heat treatment conditions

Steel	Austenitising	Tempering
13Cr (A)	980°C, OQ	610°C
13Cr (B)	1 h at 950°C, OQ	2 h at 580°C, WC
13–1	1 h at 950°C, OQ	2 h at 600°C, WC
13–4	3 h at 1000°C, OQ to 300°C, then AC	7 h at 580°C, AC +7 h at 570°C, FC +7 h at 550°C, FC
16–4	1020°C, OQ	~580°C
17–4 PH	0·5 h at 1040°C, OQ	4 h at 595°C, AC

OQ oil quenched, WC water cooled, AC air cooled; FC furnace cooled

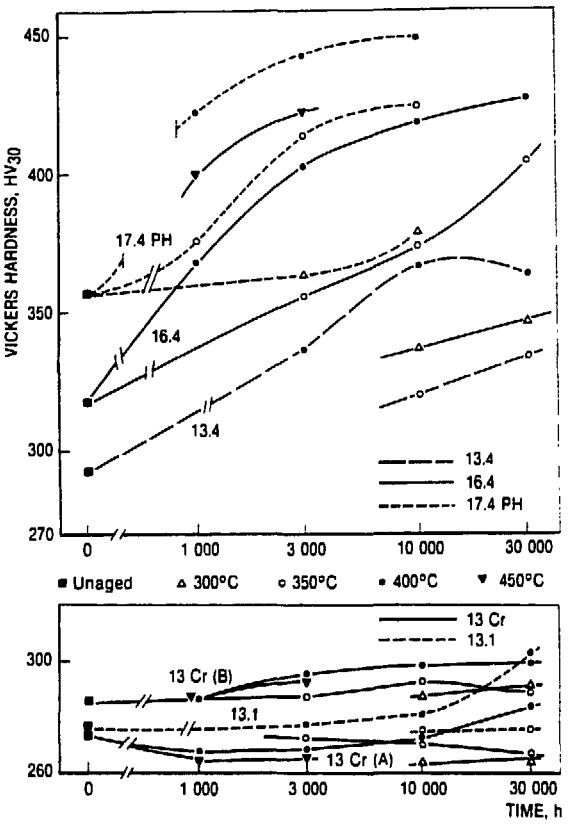

1 Variation of Vickers hardness (30 kg load) as function of time at various aging temperatures

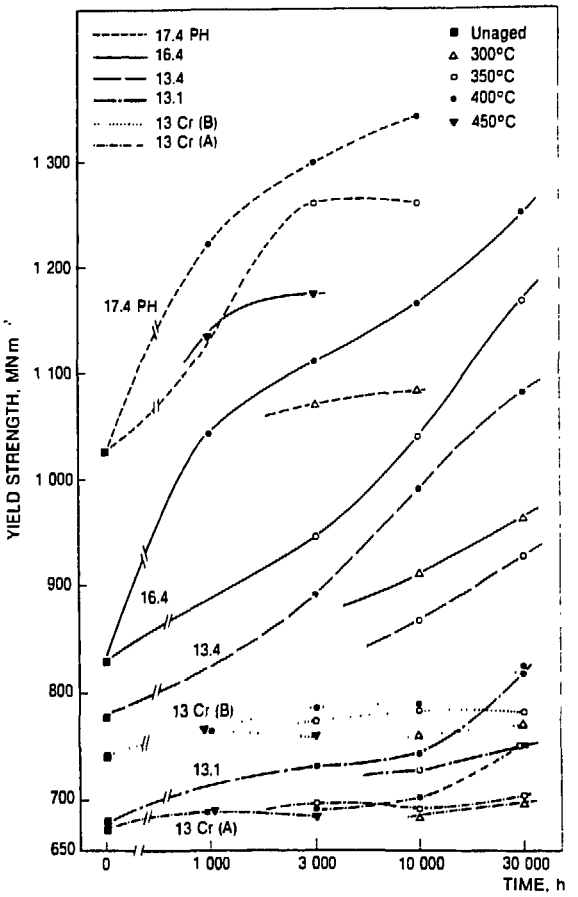

2 Variation of 0·2% yield stress as function of time at various aging temperatures

Results of aging tests

AGING TREATMENTS

The aging treatments were carried out for 1000–30 000 h between 300 and 450°C (Table 5). Note that treatments of 70 000 h are currently in progress at EDF.

MECHANICAL PROPERTIES IN VARIOUS AGING CONDITIONS

For each aging state, the Vickers hardness, yield stress, ultimate tensile strength, reduction of area, rupture elongation, Charpy V-notch impact energy transition curve, fracture appearance transition temperature ($FATT_{50}$), and upper shelf energy (USE) were determined. All the individual results are given in Ref. 10.

Hardness and tensile tests

The variation of hardness, yield stress, and reduction of area as a function of aging time at the different temperatures is shown in Figs. 1–3. The variation of ultimate tensile strength is exactly parallel to that of yield stress.

All the materials studied exhibit some age hardening, their order of increasing age hardening susceptibility being: 13Cr, 13–1, 13–4, 17–4 PH, 16–4. In the plain 13Cr and 13–1 steels, appreciable hardening (increase of Vickers hardness, yield stress, and ultimate tensile strength and decrease of reduction of area) is observed only after a 30 000 h hold at 400°C, whereas, in all the other materials, hardening is observed at all aging temperatures investigated. Aging susceptibility increases with increasing time and

Table 3 Summary of microstructure in initial quenched and tempered condition

Steel	Tempering temperature, °C	Grain size (ASTM no.)	δ ferrite		Reverted austenite volume fraction, %	Precipitates		Remarks
			Volume fraction, %	Composition, wt-%		$M_{23}C_6$	Others	
13Cr (A)	610	7–8	0·3–0·7	15·6%Cr, 0·08%Ni, 0·05%Mo	0	Yes	. .	δ ferrite located in darkly etched bands enriched in ferrite forming elements
13Cr (B)	580	6	0	...	0	Yes	$M_2(C,N)$	. .
13–1	600	5	0	. .	0	Yes		...
13–4	580	4	0	...	9·2	Yes	.	.
16–4	580	.	10–15	19·5%Cr, 2·4%Ni, 1·8%Mo	8·3	Yes	...	...
17–4 PH	595	11–12	0	. .	6·2	Yes	Nb(C,N), ε(Cu)	Darkly etched bands enriched in Cu, Ni, and P

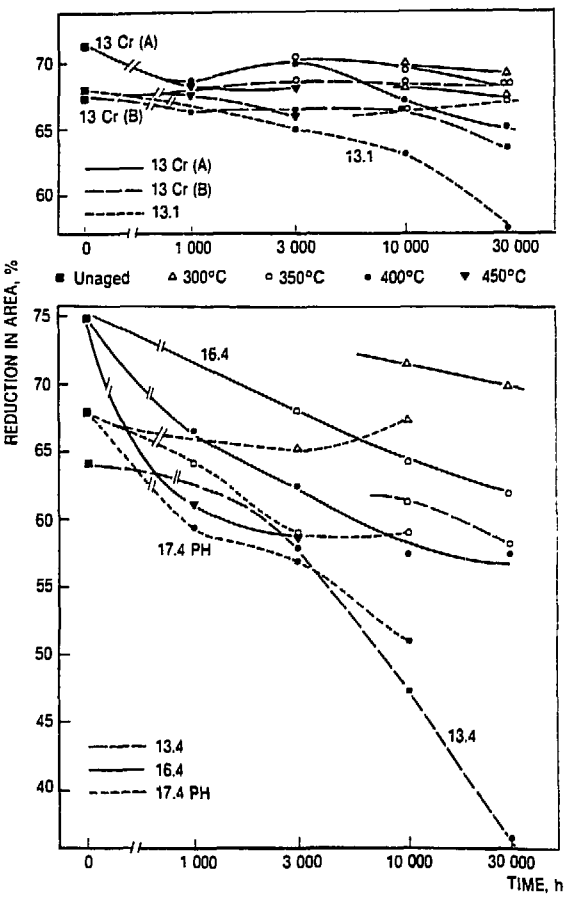

3 Variation of reduction of area as function of time at various aging temperatures

temperature (≤400°C) and with increasing chromium and molybdenum contents. Maximum hardening is not completely attained within the longest time periods investigated at 400°C (10 000 or 30 000 h depending on the steel considered); however, the maximum hardness attainable at this temperature, as estimated by extrapolating the curves of Fig. 1, is not much greater than the highest measured value (Table 6). On the other hand, at 450°C, hardening is less than at 400°C, the maximum is attained much sooner (between 1000 and 3000 h), and some subsequent overaging seems to take place. The apparent maximum of the yield strength of the 17–4 PH steel after aging for 3000 h at 350°C is entirely due to experimental scatter, and has not been observed in another heat of the same grade of steel, which was also studied (though not reported here).

The hardening ΔHV_{30} is linearly correlated with the increase of yield stress or ultimate tensile strength ΔS (*see* Fig. 4); the empiric relationship found between ΔHV_{30} and ΔS (in MN m^{-2}) is

$$\Delta S = 3{\cdot}4\Delta HV_{30} \pm 50 \quad \ldots\ldots\ldots\ldots\ldots\ldots \quad (1)$$

On the other hand, the ductility decreases steadily with aging, concomitantly with the observed hardening. It is particularly high for the 13–4 steel (Fig. 3) at 400°C and seems to reveal the occurrence of an additional mechanism of embrittlement superimposed on that due to hardening.

Table 5 Aging treatments

Temperature, °C	Time, h: 1000	3000	10 000	30 000	70 000 (in progress)
300	...	●	+ ●	+	+ ○
350	●	+ ●	+ ○ ●	+ ○	+ ○
400	+ ●	+ ○ ●	+ ○ ●	+ ○	...
450	+	+	...	...	...

+ 13Cr and 16–4; ○ 13–1 and 13–4; ● 17–4 PH.

Charpy V-notch impact energy transition curve

The transition curve and the $FATT_{50}$ temperature were determined for each aging condition; only the evolution of the $FATT_{50}$ shift ($\Delta FATT$) after aging at 400°C is shown in Fig. 5. For all conditions, the USE decreases linearly with the increase of transition temperature. For example, the Charpy energy transition curves of the most embrittled states of each steel are shown in Fig. 6.

According to Fig. 5, maximum embrittlement seems not to have been attained for any material. The rate and intensity of the embrittlement in terms of $FATT_{50}$ shift are ranked in the same order as for hardening, with the exception of the 17–4 PH and 13–4 steels, which are more embrittled than would have been expected from the hardening results. This indicates the occurrence of an additional non-hardening embrittlement mechanism.

Behaviour of each grade

With respect to the mechanical properties, the individual behaviour of each grade may be summarised in the following way.

Plain 13%Cr steel Up to 30 000 h at temperatures less than or equal to 350°C, aging is negligible. At 400°C, very little aging is observed up to 10 000 h, but it becomes significant after 30 000 h ($\Delta FATT_{max} = 30$°C).

13Cr–1Ni steel An appreciable degree of aging is observed after 30 000 h at 350°C and 10 000 h at 400°C; it evidently increases after 30 000 h at 400°C ($\Delta FATT_{max} = 93$°C).

13Cr–4Ni, 16Cr–4Ni, and 17–4 PH steels These three steels age considerably at all the temperatures investigated. The highest Charpy transition temperatures are obtained for the 17–4 PH steel, which seems the most susceptible to aging embrittlement, especially at 400°C ($\Delta FATT_{max} =$ 352°C after only 10 000 h).

Table 4 Mechanical properties in initial condition

Steel	Tempering temperature, °C	Hardness, HV30	Tensile properties: 0·2% YS, MN m^{-2}	UTS, MN m^{-2}	El, %	RA, %	Charpy V-notch impact toughness: At 20°C, daJ cm^{-2}	USE, daJ cm^{-2}	$FATT_{50}$, °C
13Cr (A)	610	273	675	825	20	71	5·5	22·6	48
13Cr (B)	580	285	740	890	20	67	2·7	16·6	85
13–1	600	275	675	825	21	68	14·0	16·1	−14
13–4	580	293	780	885	21	64	17·7	19·3	−86
16–4	580	318	830	950	23	75	23·2	28·7	−65
17–4 PH	595	355	1030	1090	19	67	20·3	22·0	−37

YS yield stress; UTS ultimate tensile strength; El elongation; RA reduction of area; USE upper shelf energy; $FATT_{50}$ fracture appearance transition temperature.

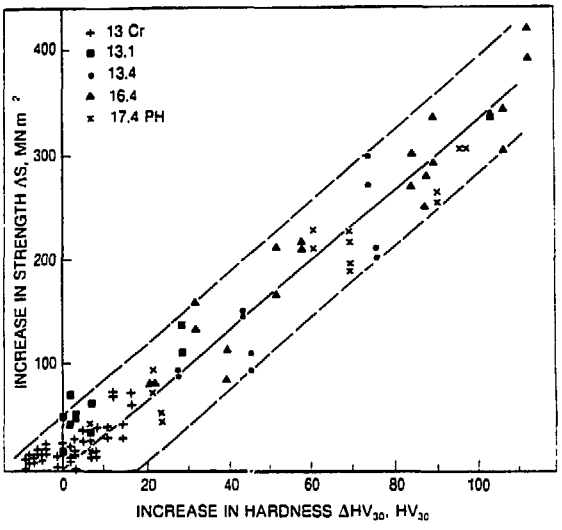

4 Relationship between increase of yield stress or ultimate tensile strength ΔS and Vickers hardness ΔHV_{30} in various aging conditions studied

Discussion

CORRELATIONS BETWEEN EMBRITTLEMENT AND HARDENING

For all the steels and almost all the aging treatments studied, there is a linear correlation between the decrease of impact energy properties ΔFATT and ΔUSE and hardening measured in terms of Vickers hardness ΔHV or yield stress and ultimate tensile strength ΔS. Figures 7–9 show these correlations. The empiric relationships obtained are:

(i) for 17–4 PH steel

$$\Delta FATT = 2{\cdot}5\Delta HV_{30} \quad . \quad . \quad . \quad . \quad . \quad . \quad . \quad . \quad . \quad . \quad (2)$$

$$\Delta FATT = 0{\cdot}75\Delta S \quad . \quad . \quad . \quad . \quad . \quad . \quad . \quad . \quad . \quad . \quad (3)$$

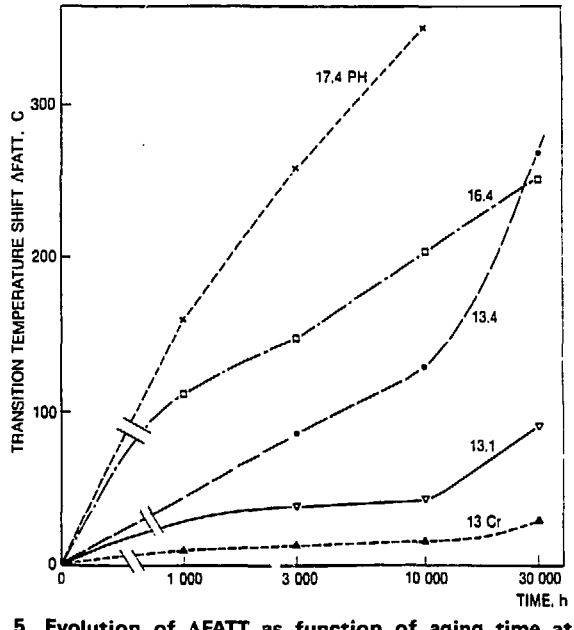

5 Evolution of ΔFATT as function of aging time at 400°C for various steels studied

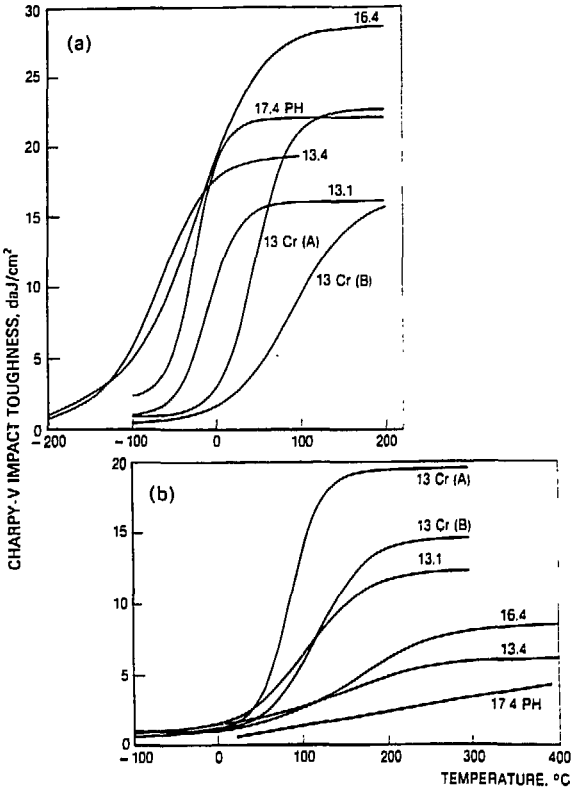

a unaged; *b* in most embrittled condition studied, i.e. 30 000 h at 400°C for all materials except 17–4 PH (aged 10 000 h at 400°C)

6 Charpy V-notch impact toughness transition curves of various steels studied

(ii) for the other steels

$$\Delta FATT = 2\Delta HV_{30} \quad . \quad . \quad . \quad . \quad . \quad . \quad . \quad . \quad . \quad . \quad (4)$$

$$\Delta FATT = 0{\cdot}60\Delta S \quad . \quad . \quad . \quad . \quad . \quad . \quad . \quad . \quad . \quad . \quad (5)$$

(iii) for all steels

$$\Delta USE = -0{\cdot}16\Delta HV_{30} \pm 2{\cdot}5 \quad . \quad . \quad . \quad . \quad . \quad . \quad (6)$$

with ΔFATT in °C, ΔS in MN m^{-2}, and ΔUSE in daJ cm^{-2}. In itself, the existence of these correlations shows that age hardening is responsible for the embrittlement of the steels in the corresponding aging conditions.

DEPARTURE FROM CORRELATION BETWEEN EMBRITTLEMENT AND HARDENING

17–4 PH steel (except after aging for 3000 and 10 000 h at 400°C)

Embrittlement of the 17–4 PH steel, except when aged for 3000 and 10 000 h at 400°C, is slightly stronger, for a given hardening, than that of the other products, especially the

Table 6 Maximum increase of hardness obtained on aging

Steel	Highest measured increase of hardness, HV30	Estimated maximum increase of hardness, HV30	Estimated time for maximum hardness, h
13Cr (A)	12	18?	>30 000
13Cr (B)	16	18?	⩾30 000
13–1	28	?	>30 000
13–4	73	75	10 000–30 000
16–4	111	115	⩾30 000
17–4 PH	95	100	⩾10 000

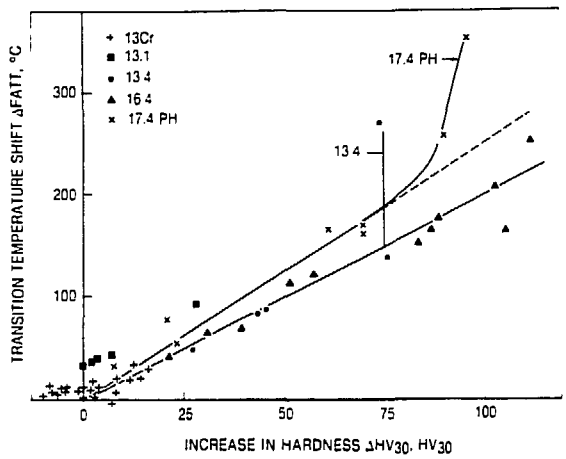

7 Relationship between transition temperature shift and hardening of steels studied in all aging conditions

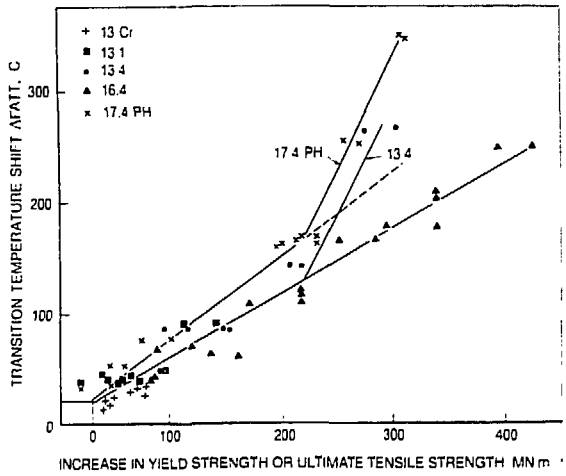

8 Relationship between transition temperature shift and tensile hardening ΔS (= ΔYS or ΔUTS) of steels studied in all aging conditions

16–4 steel, although the hardening kinetics of these two steels is very similar (Figs. 1 and 2). This shows that the hardening mechanism of the 17–4 PH steel is identical to that of the other steels (α' precipitation: *see* below). In particular, there is no additional copper precipitation during the aging treatments, although these have been carried out below the tempering temperature. Therefore, the observed increase of embrittlement associated with a given hardening probably results from the enhancing effect of the higher tensile properties and reduced ductility, due to copper precipitation, on the embrittlement induced by α' precipitation.

Aging states 3000 and 10 000 h at 400°C for 17–4 PH steel and 30 000 h at 400°C for 13–4 steel

These aging states clearly do not follow the embrittlement hardening correlations established for these steels (Figs. 7 and 8). The excess embrittlement in terms of ΔFATT is about 100°C for the 13–4 steel aged 30 000 h at 400°C and 120 and 50°C for the 17–4 PH steel aged, respectively, 10 000 and 3000 h at 400°C.

Microfractographic examinations have been carried out on Charpy specimens broken just at the beginning of the transition region on the Charpy transition curve and others broken just at the end of it.

In the initial condition the two steels exhibit very little intergranular brittle fracture (0% for the 17–4 PH steel and 5% for the 13–4 steel). In the hardest correlated aged state (10 000 h at 350°C for the 17–4 PH steel and 10 000 h at 400°C for the 13–4 steel), there is, respectively, some (35%) and virtually no (3%) intergranular fracture at the start of the transition. Conversely, the uncorrelated states exhibit a significant amount – between 60 and 95% – of intergranular brittle or ductile (depending on test temperature) fracture, as shown in Fig. 10.

Previous work has shown that these types of steel are subject to reversible temper embrittlement caused by intergranular segregation of phosphorus during long term aging of 13–4,[7,8] plain 13%Cr,[5] and 13–1[6] steels at 400°C or higher temperatures. The observed behaviour of the 17–4 PH and 13–4 steels is consistent with both the phosphorus contents (the highest: 0·022 and 0·025%, respectively) and the negligible or low molybdenum contents of the two steels (0·06 and 0·57%, respectively).

The calculation of the transition temperature shifts due to this mechanism[10] gives a good approximation of the measured values. This estimation is conservative and shows that such an embrittlement process (reversible temper embrittlement) is not expected for the steels studied (given their phosphorus and molybdenum contents) in the service conditions of PWR components (i.e. up to 300 000 h) at temperatures equal to or below 300°C.

It should be noted that the plain 13%Cr steels studied already exhibit a strong intergranular brittleness in the initial condition. However, this brittleness does not evolve on aging at the temperatures investigated; it is probably due to temper embrittlement already induced during the tempering treatment.

METHOD OF PREDICTION OF MAXIMUM EMBRITTLEMENT INDUCED BY AGING AT TEMPERATURES UP TO 400°C

As in ferritic stainless steels, the embrittlement observed in low carbon martensitic stainless steels is due to the very fine precipitation of chromium rich α' phase in the tempered martensite and in the δ ferrite when present. Its lattice is

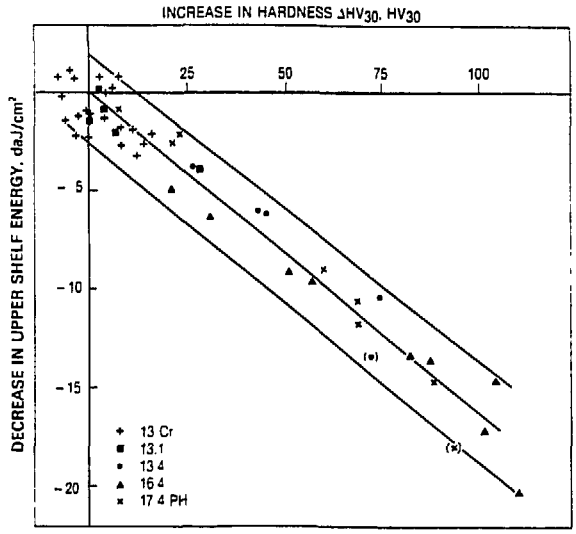

9 Relationship between decrease of upper shelf energy and hardening of steels studied in all aging conditions

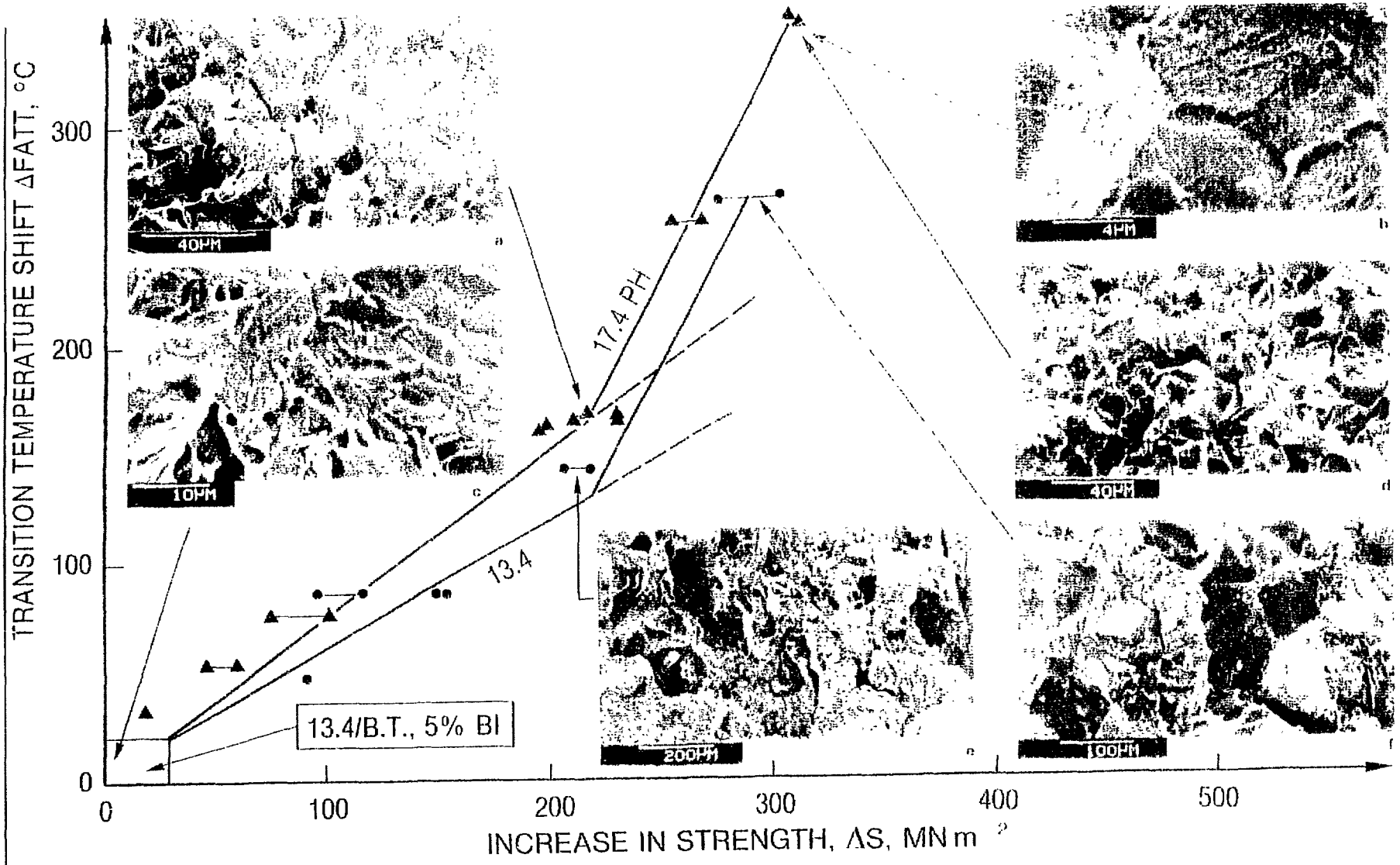

%BI, %DI percentage of brittle intergranular or ductile intergranular fracture
a 17 4 PH, BT, 35%BI *b* 17 4 PH, ET, 60%DI, *c* 17 4PH BT, 0%BI, *d* 17 4 PH BT, 95%BI, *e* 13 4 BT, 3%BI / 13 4, BT, 60%BI

10 **Relationship between transition temperature shift and tensile hardening ΔS of 13 4 and 17 4 PH steels, associated with fractographic appearance of some Charpy V-notch specimens fractured at beginning (BT) and at end (ET) of transition zone**

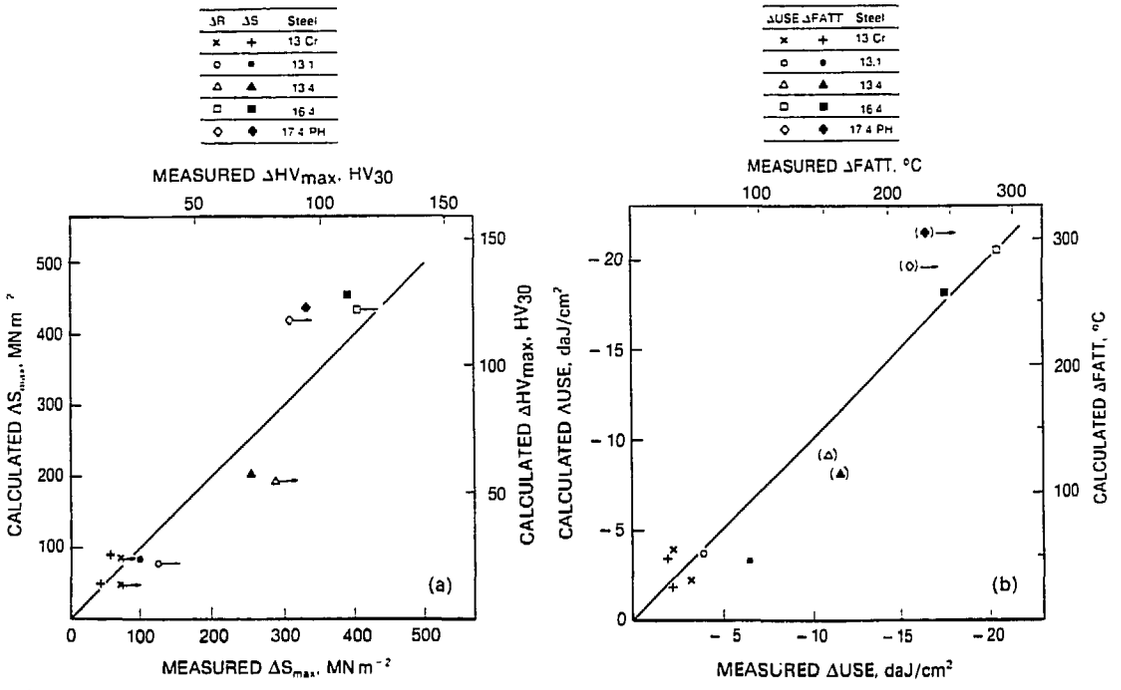

for symbols with arrow, abscissa at base of arrow (symbol) corresponds to highest measured property and that at arrowhead corresponds to estimated maximum; symbols in parentheses are deduced from measured values by extrapolating to zero temper embrittlement (*see* Figs. 7–9)

11 Relationship between calculated and measured maximum variations of mechanical properties obtained on aging of steels studied

bcc and includes some iron (5–10%) and molybdenum.[3] Depending on fabrication conditions, this precipitation is homogeneous or heterogeneous on dislocations. The hardening power of the homogeneous precipitation can become very great. Microstructural study of industrial grades in various aged conditions[3,4] has shown that, at 400°C, α' precipitation is homogeneous, whereas, at 450°C, it is partially dislocation controlled.

The results of the present study are in good agreement with those of Meyzaud and co-workers[3,4] concerning the influence of chemical composition (chromium, molybdenum, and carbon contents) and of microstructure (reverted austenite content) on the aging response of these materials. On the other hand, the present authors have shown that the maximum hardening is not attained even after 30 000 h at 400°C, whereas they[3,4] claim that maximum hardening is attained already after 5000–10 000 h at 400°C. Replotting their results in the same (logarithmic) coordinates as those used here shows that this is not true.[10] Similarly, using the $FATT_{50}$ criterion to account for embrittlement is better than using half the upper shelf energy (cf. Refs. 3 and 4) for high embrittlements, due to the absence, in this instance, of an observed upper shelf (*see* Fig. 6). In this respect, too, using a superior criterion shows that maximum embrittlement is not attained even after 30 000 h at 400°C.

Therefore, the method of prediction proposed in Refs. 3 and 4 has been modified as follows. If ΔHV_{max} denotes the maximum hardening estimated in the present work for the materials investigated (*see* Table 6), a new derivation is obtained

$$\Delta HV_{max} = [23{\cdot}8 - 0{\cdot}34(\%\gamma)](Cr^* - 10{\cdot}2) \quad . \quad . \quad . \quad . \quad (7)$$

where

$$Cr^* = \%Cr + \%Mo - A\,(\%C)$$

Here $\%\gamma$ is the volume fraction of austenite which does not age harden, 10·2 is the solubility limit of Cr* in wt-%, Cr* is the chromium plus molybdenum content in solid solution, and A is a coefficient dependent on carbide type:

(i) $A = 16$ for $M_{23}C_6$ only: 13Cr (A), 13–1, 13–4, 16–4
(ii) $A = 12$ for $\frac{3}{4}$ of $M_{23}C_6$ and $\frac{1}{4}$ of $M_2(C,N)$: 13–Cr (B)
(iii) $A = 8$ for half of the carbon content in $M_{23}C_6$ and half in Nb(C,N): 17–4 PH.

The maximum variations of the other properties can be calculated using equations (1), (2), (4), and (6). Figure 11 shows the comparison between measured and calculated values. They are generally in good agreement: only the predictions for mechanical property evolution for the 13–4 steel are somewhat underestimated.

The behaviour of the 16–4 steel, which contains 10–15% δ ferrite, is slightly different from that of the other materials – between 10 000 and 30 000 h at 400°C, the hardening continues to increase, whereas it increases very little after 3000 h at this temperature in the other steels. This effect arises from the presence of δ ferrite, since this phase continues to harden while the hardening of tempered martensite seems to saturate after 10 000 h at 400°C, as shown by measurements of microhardness (Fig. 12). This is in agreement with the observations of Refs. 3 and 4, which showed that α' precipitation in industrial steels was essentially heterogeneous at 450°C and homogeneous at 400°C, whereas it was homogeneous at both temperatures in laboratory heats. In effect, the latter materials differ from industrial products because of their lower dislocation density, which favours the hardening homogeneous precipitation. In the 16–4 materials studied here, the greater ability of ferrite to age harden compared with tempered martensite is due to its higher chromium content (20% compared with 16%; Table 3) and to its much lower dislocation density, as with the laboratory heats. For high alloy steels having, a higher δ ferrite content, extra hardening, probably associated with additional embrittlement, is expected between 10 000 and 100 000 h at 400°C.

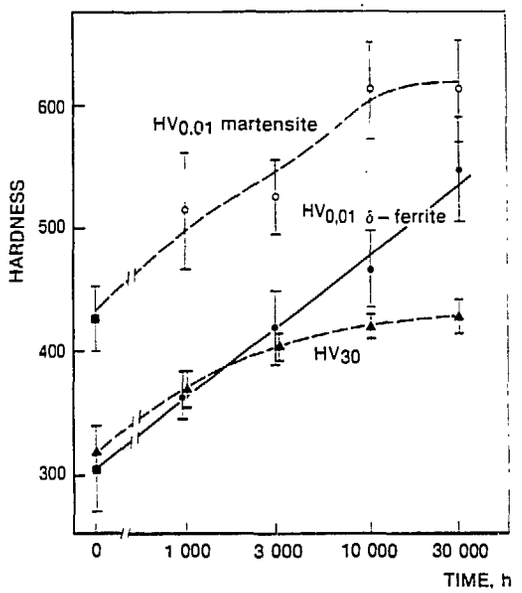

12 Evolution of Vickers microhardness (10 g load) of δ ferrite and of tempered martensite, compared with average Vickers hardness (30 kg load) of 16–4 steel, as function of aging time at 400°C

METHOD OF PREDICTION OF STEEL PROPERTIES AS FUNCTION OF AGING PARAMETERS

Time–temperature equivalence curves

When possible (i.e. only for the 13–4, 16–4, and some 17–4 PH steels), the curves of iso-variation of the mechanical properties have been plotted in a $(1/T)$–$\log t$ diagram. Figure 13 shows the iso-Charpy V-notch impact energy at room temperature for the 16–4 steel. This plot allows the average apparent activation energies to be determined. The aging kinetics of these products may now be described using a parameter $P(t, T)$ based on an Arrhenius type relationship

$$P(t, T) = \log t + 0{\cdot}43(Q/R)(1/T_o - 1/T) \quad . \quad . \quad . \quad . \quad . \quad (8)$$

where

t = aging time (in hours) at temperature T (in kelvin)
R = gas constant (8·31 J K^{-1} mol^{-1})
Q = apparent activation energy (in J mol^{-1})

An average value of $Q = 160$ kJ mol^{-1} in the range 300–400°C has been estimated for all steels except the

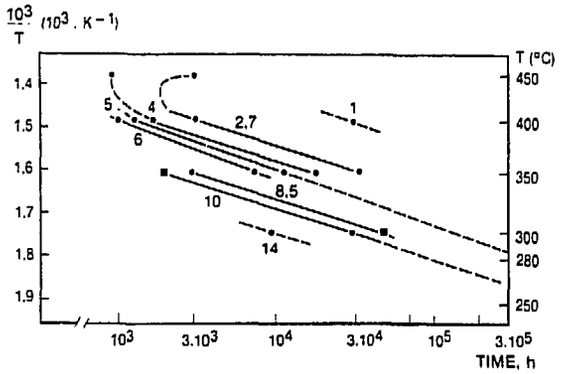

13 Iso-Charpy V-notch impact toughness curves of 16–4 steel in $(1/T)$–log t coordinates; numbers on curves indicate corresponding toughness in daJ cm^{-2}

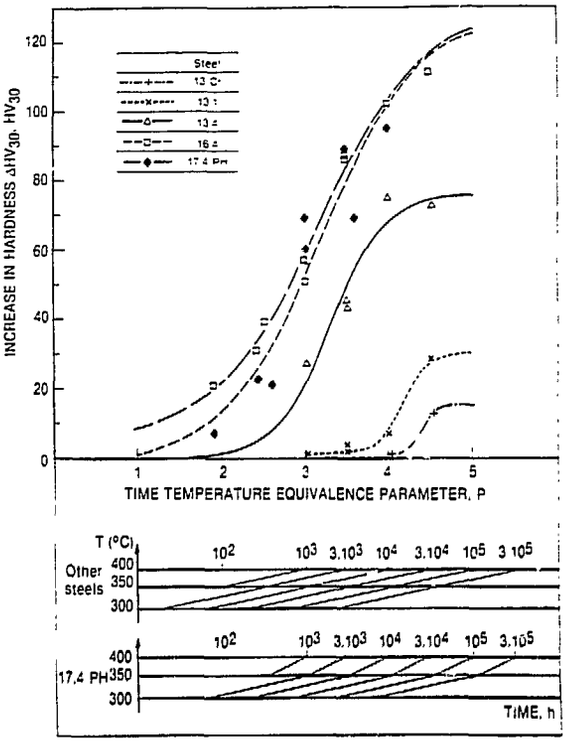

symbols are measured values; curves are plotted according to equation (11)

14 Evolution of hardening ΔHV_{30} as function of time–temperature equivalence parameter $P(t, T)$

17–4 PH, for which two energies seem to be effective, depending on aging temperature. The following relationships give the parameter P:

(i) 17–4 PH steel

$$\left.\begin{aligned} P' &= \log t + 0{\cdot}43\,\frac{55\,000}{R}\left(\frac{1}{673} - \frac{1}{T}\right) \\ &\qquad 350°C \leqslant T \leqslant 400°C \\ P &= P'(350°C) + \frac{160\,000}{R}\left(\frac{1}{623} - \frac{1}{T}\right) \\ &\qquad 300°C \leqslant T \leqslant 350°C \end{aligned}\right\} \qquad (9)$$

(ii) other steels

$$P = \log t + 0{\cdot}43\,\frac{160\,000}{R}\left(\frac{1}{673} - \frac{1}{T}\right)$$

$$300°C \leqslant T \leqslant 400°C \quad . \quad . \quad . \quad . \quad . \quad . \quad . \quad (10)$$

In the absence of other data, this last formulation will also be used for the plain 13Cr and 13–1 steels.

As usual, the values of activation energy determined are underestimates at the lower aging temperature because of the curvature of C curve kinetics.[11] As a result, the extrapolations to the lower temperatures (i.e. below 300°C) based on equations (9) and (10) will be conservative.

Table 7 Values of parameters in equation (11) used to plot curves of Fig. 14

Steel	ΔH_o, HV30	ΔH_1, HV30	P_o	P_1	$\Delta H_1/P_1$
16–4	70	60	3·25	1·21	50
17–4 PH	64	66	3·21	1·20	55
13–4	38.	38	3·31	0·64	59
13–1	16	15	4·17	0·29	52
13Cr	7	7	4·38	0·13	54

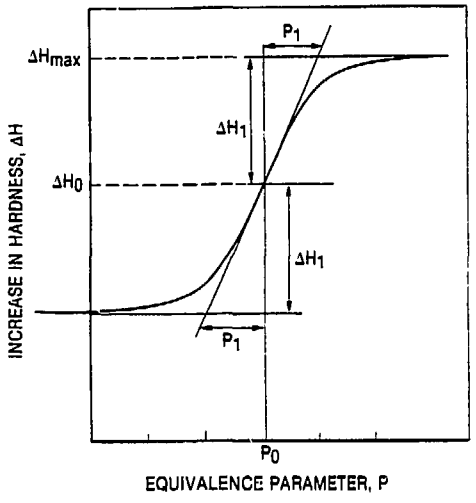

$y = \tanh x$, where $y = (\Delta H - \Delta H_0)/\Delta H_1$ and $x = (P - P_0)/P_1$

15 Definition of parameters of equation (11), which describes curves in Fig. 14

Materials		Present results: Tempering temperature (°C)	Results of ref 4: Tempering temperature (°C)
13 Cr	+	610	–
13 1	×	600	–
13 4	△	590	600
16 4	□	580	620, 550
17 4 PH	◆	595	600

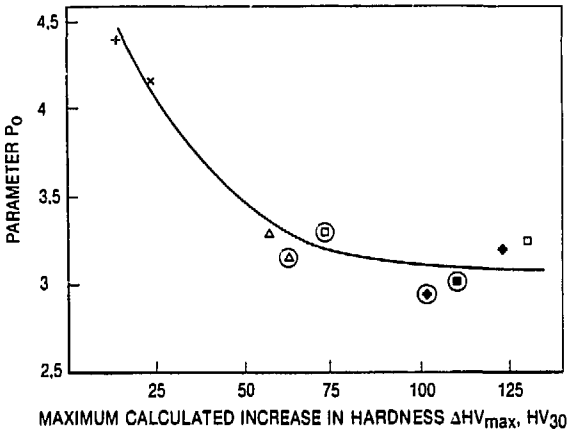

16 Relationship between P_0 (equivalent time for half maximum hardening in Fig. 14) and maximum hardening ΔHV_{max} calculated using equation (7)

Generalisation

The above results enable the principle of a global prediction of the mechanical properties of martensitic stainless steels during aging at temperatures up to 400°C to be derived.

Figure 14 shows the evolution of the hardening ΔHV_{30} of the various steels studied as a function of the equivalence parameter P. The curves obtained are sigmoid and have been adjusted on experimental points using the following relationship (the parameters are defined on Fig. 15)

$$\Delta HV = \Delta H_0 + \Delta H_1 \tanh\left(\frac{P - P_0}{P_1}\right) \quad \ldots\ldots (11)$$

The values of these parameters are given in Table 7. The values of maximum hardening ΔHV_{max} used* to calculate these parameters correspond to aging treatments at 400°C; if the values of the highest hardening level differed greatly between one temperature and another, the time–temperature equivalence would not apply. However, considering the activation energies obtained above, aging at temperatures less than 350°C for times of the order of the service life of nuclear power plant (~300 000 h) leads to a value of P less than 4. Therefore, representative aging treatments correspond to points to the left of the upper shelf of the curves in Fig. 14, and this transition zone of the curves, which is validated by experimental points, is not affected greatly by the height of the upper shelf. Therefore, it is possible to use these curves to predict the mechanical properties of martensitic stainless steel after aging for a given time at a given temperature.

For this, it is necessary to calculate P using equations (9) and (10) and build the curve $\Delta HV = f(P)$, i.e. equation (11), specific to the steel; the variations of the other properties are then derived from equations (1)–(6). The parameters in equation (11) are determined in the following way. In practice, $\Delta H_0 \approx \Delta H_1 \approx \Delta HV_{max}/2$, where ΔHV_{max} is calculated on the basis of the metallurgical parameters of the steel by means of equation (7). The slope of the curves at the point of inflexion $\Delta H_1/P_1$ is independent of the material considered (*see* Table 7) and, hence, 54 can be selected as an average value. Now, since ΔHV_{max} and $\Delta H_1/P_1$ are known, P_1 is easily derived. It remains to evaluate the abscissa P_0 of the inflexion point of the sigmoid curve for the steel considered. Now, P_0 decreases with increasing Cr* because chromium supersaturation in the solid solution is the driving force for α' precipitation (Fig. 16); as the driving force increases, the equivalent time P_0 for completion of half the hardening reaction decreases. It is proposed to use the experimental relationship between P_0 and ΔHV_{max} (Fig. 16), because this quantity takes into account the influence of microstructural parameters (austenite content, implicitly tempered martensite structure, precipitation, etc.) on the hardening. This curve is well approximated by the following numerical expression

$$P_0 = 4{\cdot}65 + 10{\cdot}68(\Delta HV_{max})^{-0{\cdot}918} - 0{\cdot}367 \ln(\Delta HV_{max}) \quad \ldots\ldots (12)$$

However, the coefficients of equation (7) are averages empirically established over all the steels studied and, thus, cannot account for the microstructural features specific to each steel, which explains the scatter observed in Fig. 16. Finally, equation (11) becomes

$$\Delta HV = (\Delta HV_{max}/2)\{1 + \tanh[108(P - P_0)/\Delta HV_{max}]\} \quad \ldots\ldots (13)$$

Note that, when reversible temper embrittlement occurs, its contribution must be added to the variations of properties which are due to α' precipitation and are calculated on the basis of equations (2), (4), and (6).

Application of this method of prediction to materials studied

This method has been applied to all the materials studied here in all aged conditions for aging temperatures below or equal to 400°C, and the properties thus calculated have been compared with the measured values. The comparison is shown in Fig. 17 for hardness, tensile, and impact toughness properties. The data points in parentheses correspond to the aging conditions leading to reversible temper embrittlement, the contribution of which is not taken into account in the prediction. As expected, this phenomenon affects essentially the impact transition temperature, the upper shelf energy much less, and the room temperature tensile properties not at all. Except for these

*When the maximum hardening ΔHV_{max} was not experimentally known, a value was selected equal to the calculated value.

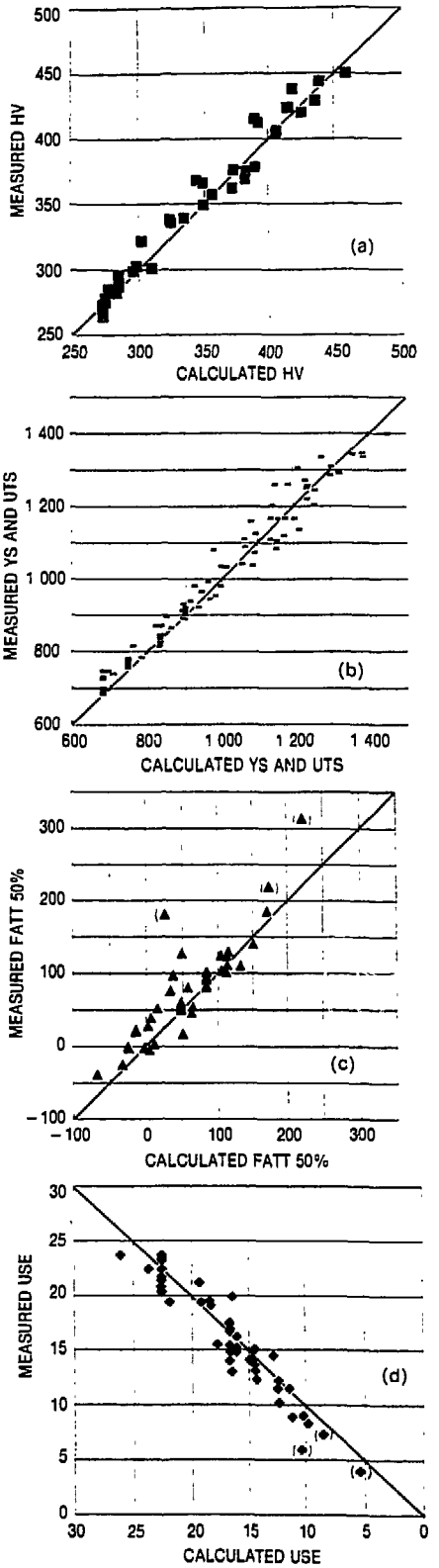

a Vickers hardness; *b* tensile properties; *c* $FATT_{50}$; *d* USE
symbols in parentheses correspond to aging conditions where strong reversible temper embrittlement (RTE) has been identified (equations used predict embrittlement associated with α' precipitation induced hardening. RTE is not taken into account)

17 Correlation between measured values of mechanical properties and values predicted using equations (13), (2), (4), and (6) for aged materials

well identified temper embrittled conditions, the agreement between predicted and measured values is very good for hardness, yield stress, and tensile strength. The data are slightly more scattered for the impact transition temperature and upper shelf energy, where the variations are slightly underestimated in some cases; it is possible that these correspond to aging conditions where some slight temper embrittlement might have occurred and not be recognised above.

Conclusion

The aging of the martensitic stainless steels studied is essentially due to α' precipitation. It manifests itself by an increase of hardness, yield stress, and tensile strength, a concomitant decrease of tensile ductility (reduction of area and ultimate elongation), and impairment of impact properties (transition temperature and upper shelf energy). The embrittlement due to this mechanism is linearly correlated with hardening. The hardening increases with aging time and temperature up to 400°C and with the chromium and molybdenum contents in solid solution, and decreases with increasing volume fraction of non-hardenable austenite. The hardening of the δ ferrite seems to be strong and to continue after 10 000 and 30 000 h at 400°C, whereas that of the tempered martensite tends to saturate.

The 17–4 PH steel is the most embrittled of the materials studied. Some of the materials having high phosphorus and low molybdenum contents aged at 400°C exhibit some reversible temper embrittlement. However, in service conditions, i.e. up to 300 000 h at 300°C, and for all the steels studied, such an embrittlement is not expected to occur.

A general numerical method of prediction of the evolution of the mechanical properties of these steels due to α' precipitation induced by any aging treatment up to 400°C has been proposed. It is a function of the chemical composition, phase content, initial properties, and aging conditions of the steel.

References

1. H. J. NIEDERAU: *Stahl Eisen*, 1978, **98**, (4), 385–392.
2. K. C. ANTONY: *J. Met.*, 1963, **12**, 922–927.
3. Y. MEYZAUD, H. SCHAFF, R. COZAR, and J. L. CASTAGNE: *Bull. Cercle Étud. Métaux*, 1982, **14**, 19, paper 10.
4. Y. MEYZAUD and R. COZAR: in Proc. Conf. on 'Ferritic alloys for use in nuclear energy technologies', Snowbird, UT, June 1983, The Metallurgical Society of AIME, 27–35.
5. Ph. LEMBLE, A. PINEAU, J. L. CASTAGNE, Ph. DUMOULIN, and M. GUTTMANN: *Met. Sci.*, 1979, **13**, (8), 496–502.
6. R. GUILLOU, M. GUTTMANN, and Ph. DUMOULIN: *Met. Sci.*, 1981, **15**, (2), 63–72.
7. J. HUBACKOVA, K. MAZANEC, M. KOUTNIK, A. POTMESILOVA, and V. CIHAL: *Kovové Mater.*, 1986, **24**, (3), 290–301.
8. M. TSUBOTA, K. TAJIMA, H. SAKAMOTO, and T. OKADA: in 'Environmental degradation of materials in nuclear power systems – water reactors', (ed. G. J. Theus and J. R. Weeks), 731–736; 1988, Warrendale, PA, The Metallurgical Society of AIME.
9. B. YRIEIX: 'Caractérisation et étude du traitement thermique de produits corroyés en aciers inoxydables martensitiques à 13–17% de chrome', EDF Report no. HT-41/PV D 704, EDF, Moret-sur-Loing, 1989.
10. B. YRIEIX: 'Étude du vieillissement entre 300 et 450°C de produits corroyés en aciers inoxydables martensitiques à 13–17% de chrome', EDF Report no. HT-41/PV D 723-A, EDF, Moret-sur-Loing, 1989 (also Ing. CNAM thesis, Conservatoire National des Arts et Métiers, Paris, 1989).
11. S. BONNET, J. BOURGOIN, J. CHAMPREDONDE, D. GUTTMANN, and M. GUTTMANN: *Mater. Sci. Technol.*, 1990, **6**, (3), 221–229.